Proceedings of the 2020 IISE Annual Conference
L. Cromarty, R. Shirwaiker, P. Wang, eds.

Molecular Dynamics Simulations of PAA as Resist for Nanoimprint Lithography

Abstract ID: 785974

Jahlani I. Odujole, Salil Desai
Department of Industrial and Systems Engineering
North Carolina Agricultural and Technical State University
Greensboro, NC, 27411, USA

Abstract

Nanoimprinting of polymers lays the foundation for several electronic and biomedical devices. Process parameter optimization have been conducted using thermal nanoimprint (T-NIL) experimentation. However, the underlying deformation mechanism of specific polymers under varying process condition needs further exploration. This research investigates the deformation behavior of poly acrylic acid (PAA) as a thermoplastic resist material for the T-NIL process. Molecular dynamics modeling was conducted on a PAA substrate imprinted with a rigid, spherical indenter. The effect of indenter size, force, and imprinting duration on the indentation depth, penetration depth, recovery depth, and recovery percentage of the polymer was evaluated. The results show that the largest indenter, regardless of force has the most significant impact on deformation behavior. The results of this research lay foundation for explaining the effect of several T-NIL process parameters on virgin PAA thermoplastic resist material.

Keywords
Polymer; Nanoimprint; Molecular Dynamics; Indenter; Materials.

1. Introduction
Nanoimprint lithography (NIL), a high-throughput and low-cost method has demonstrated 25 nm feature sizes with 70 nm pitch, vertical and smooth sidewalls, and nearly 90° corners [1]. Enhancements in this field have improved the ultimate resolution of nanoimprint lithography to sub-10 nm. NIL offers the advantage that the imprint process is repeatable and the mold is durable for up to 500 cycles of imprinting. In addition, NIL over non-flat surfaces (3D contours) and uniformity over a 15 mm by 18 mm area has been demonstrated extending its applicability. Nanoimprint lithography has been successfully used for fabricating nanoscale photodetectors, silicon quantum-dot, quantum-wire, and ring transistors [2-4].

The two main types of NIL are: thermal nanoimprint lithography (T-NIL) and ultra-violet lithography (UV-NIL). This research employs the T-NIL method. In T-NIL, a thermoplastic resist is spin-coated onto a rigid substrate and imprinted by a rigid mold [5]. The thermoplastic resist is a polymer that exhibits unique qualities when heated up to its glass transition temperature. The substrate is typically made of a hard material such as silicon. The mold is typically comprised of silicon or silicon dioxide that has been etched using a focused ion beam (FIB). During the T-NIL process the mold is pressed into the resist at a temperature close to the polymer's glass transition temperature (T_g). After the mold is held in place for a desired duration, the temperature is decreased, and the mold is retracted from the system. After the mold removal, the polymer resist has a negative replica of the pattern that was etched onto the mold. Typically, scanning electron microscopy (SEM) is utilized to image the surface features. In addition, atomic force microscopy (AFM) is conducted to evaluate the pattern profiles and surface topography.

This research utilizes molecular dynamics simulations [6-10] to determine the ideal process parameters for NIL experiments. In traditional NIL PMMA is used as a thermoplastic resist, however newer classes of polymers have extended the applicability of NIL, poly acrylic acid (PAA) [11]. Spherical, rigid indenters with different sizes are subjected to a predetermined force to make determinations about the indentation profile, penetration depth, and recovery behavior. The findings show that PAA is a viable candidate to replace PMMA in NIL environments.

2. Methods

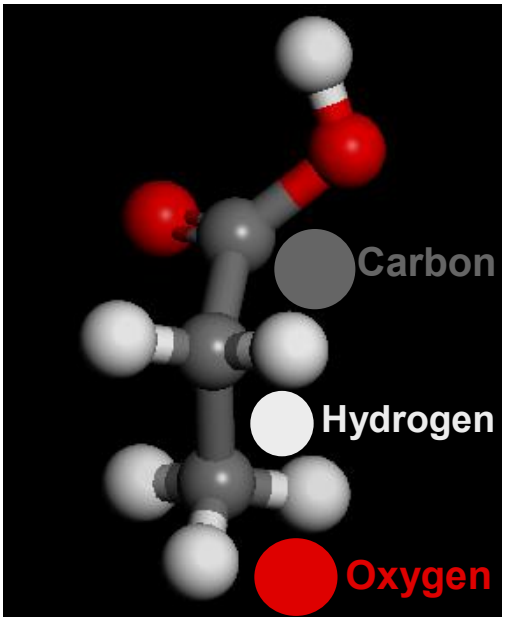

Figure 1: Molecular formulation of PAA chains

The chemical formula for PAA is $C_3O_2H_4$. The initial polymer chains were created in Materials Studio as shown in Figure 1. One isotactic chain of PAA was built replicated to form the polymer chain. There were 20 monomers per chain. This polymer chain was replicated 8 times in the horizontal plane for 7 layers, and 1 time for the bottom layer. The final atom count was 12,208. Using a Materials Studio tool called Geometry Optimization., the placement of molecules was arranged in a Newton consistent fashion. After the initial formulation of the polymer chains, the entire system was relaxed similar to [11]. Relaxation was performed to bring the system to state of thermal equilibrium [12-16]. After the initial set-up, the energy in the system was minimized over the course of 5000 time steps using the smart minimizer function in Materials Studio.

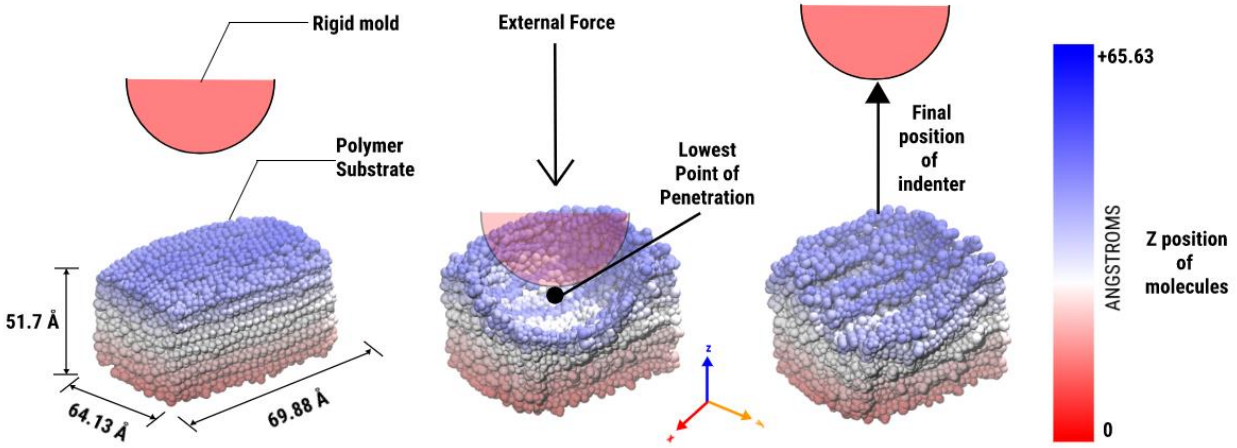

Figure 2: Schematic of overall NIL process

Molecular dynamics simulations were employed in this research to evaluate the deformation behavior of PAA using an open-source code – LAMMPS [17] and visualized in OVITO [18]. After the chains were built, the were then transferred to LAMMPS using a converter. The PAA structure was minimized additionally in the MD software to ensure equilibrium. The entire system was raised to above the glass transition temperature (135° C) of PAA. Further, the indenter was lowered onto the resist and held for a certain duration of time as seen in figure 2. After the molding phase, the entire system was cooled to room temperature and the mold was retracted. All of the deformation phases of the NIL process were analyzed using output metrics such as indentation profile to determine the effect of the indenter on the polymer material. MATLAB source code was used to develop sub-routines for the analysis on graphical processing units [19, 20].

Table: 1 CVFF Parameters for PAA polymer

Masses			
Atom	Atomic mass (amu)		
C	12.01115		
O	15.99940		
H	1.00797		
Bond parameters			
Bond type	r_0(Å)	K_B (Kcal mole^{-1})	
H-C	1.105	340.6175	
C-C	1.526	322.7158	
C-O	1.23	615.322	
Angle parameters			
Angle type	θ_0 (degrees)	K_A (Kcal mole^{-1})	
H-C-H	106.4	39.5	
H-C-C	110.0	44.4	
C-C-C	110.5	46.6	
C-C-O	120.0	68.0	
C-O-O	112.0	50.0	
H-C-O	109.5	57.0	
O-C-C	120.0	68.0	
Torsion parameters			
Angle type	ϕ_0 (degrees)	n	K_A (Kcal mole^{-1})
H-C-C-C	0	3	0.1581
C-C-C-O	0	0	0
O-C-O-C	180	2	2.25
H-C-C-O	0	1	0.1581
Van der Waals parameters			
Atom type	A	B	
C	0.389999952	3.875409636	
O	0.2280000124	2.8597848722	
H	0.38000011	2.4499714540	
Cut-off distance = 9.5 Å			

3. Results and Discussion

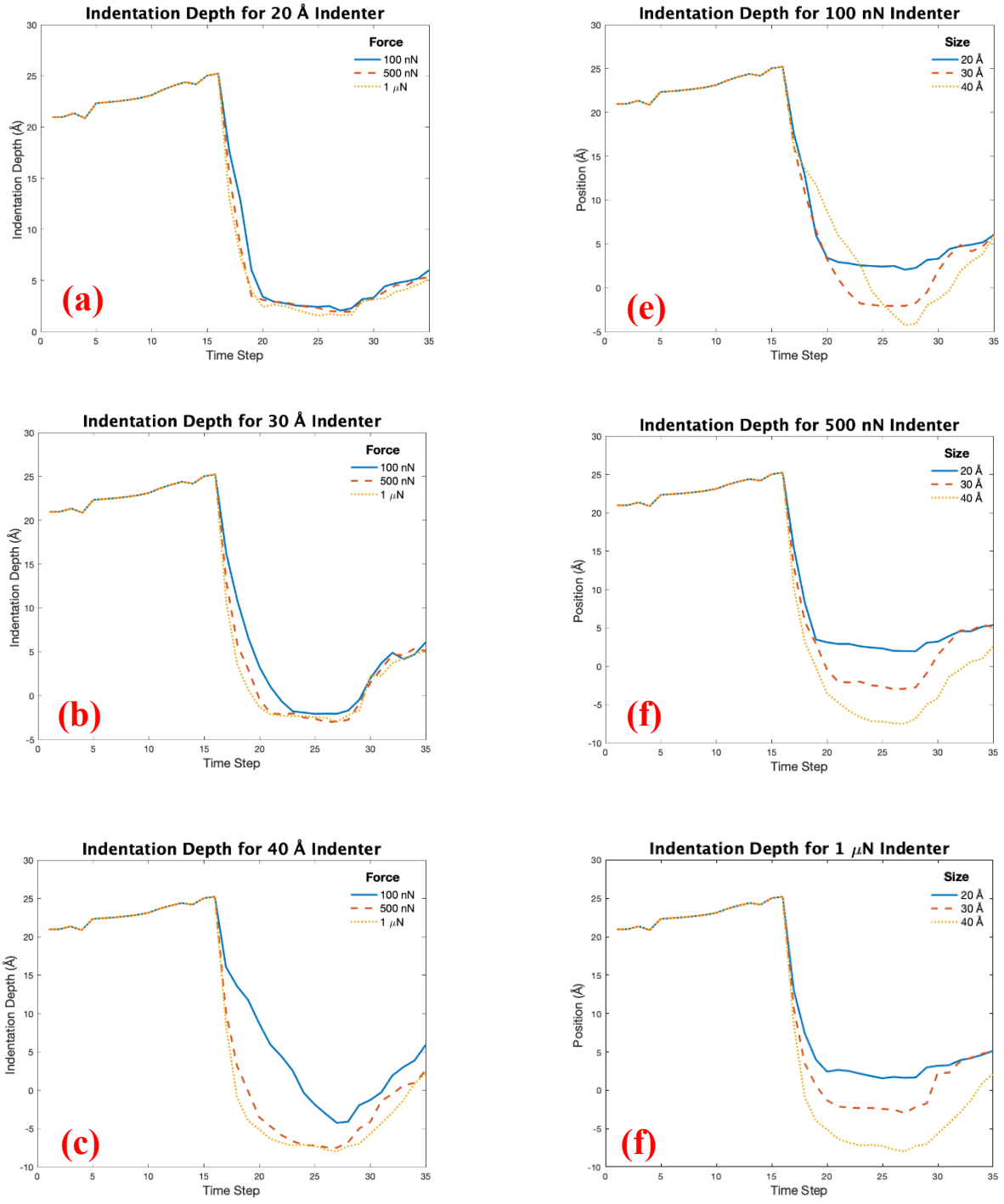

Figure 3: Indentation profile for PAA for (a) 2nm indenter (b) 3nm indenter (c) 4nm indenter (d) 100 nN indenter (e) 500 nN indenter (f) 1 µN indenter

When considering the indentation force and size of the indenter, the indenter size had more of an impact on indentation profile. The largest indenter penetrated the deepest into the resist material when indenter size was kept constant in

terms of force. For the smallest indenter, the resist experienced the lowest amount of recovery. The largest force caused similar indentation profiles for all indenter sizes as seen in figure 3(f).

Indentation depth (I_d) is determined by the distance that a group of surface atoms move from their original position as demonstrated in figure 3. In this case the I_d is graphed and analyzed over the span of the entire simulation, frame by frame. The overall trends showed that for higher force and larger indenters, the indentation deformation was significant. For example, in the figure for 1 μN of force, the 4nm indenter caused the surface atoms to descend to the lowest point compared to the other indenters. The indentation behavior was most consistent with the model is for the 40-angstrom indenter. The surface molecules descended to their lowest position and recovered to plateau region where permanent material deformation occurs as seen in figure 4.

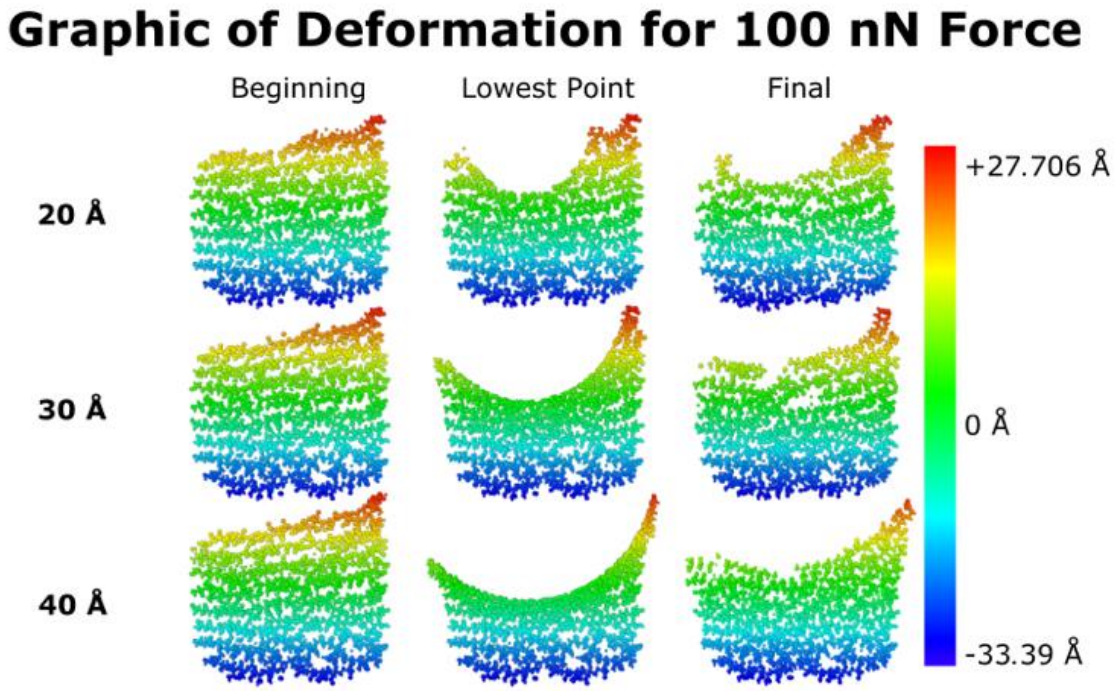

Figure 4: Cross-sectional view of indentation force of 100 nN

4. Conclusion

Viscoelastic materials including PAA are excellent candidates for the NIL process since they provide a viable substitute to PMMA. The effect of indenter size and applied force on virgin PAA was evaluated based on in terms of the indentation profile. Larger indenter sizes (40 angstrom and 30 angstrom) had deeper indentation profiles and high recovery rates. The 40-ansgtrom indenter with a 1 μN of force caused the surface molecules to descend to the lowest point compared to the other indenters. Varying indenter force and size can provide insight into the feasibility of the application of this material. The molecular model developed in this research will be expanded to include other polymers such as polystyrene.

Acknowledgements

This research was supported by U.S Dept. of Education Title III HBGI Fellowship. The authors would like to express their gratitude for funding support from the National Science Foundation Grant (NSF CMMI Award #1663128) and the Center of Excellence in Product Design and Advanced Manufacturing (CEPDAM) at North Carolina A&T State University.

References

[1] S. Y. Chou, P. R. Krauss, and P. J. Renstrom, "Imprint of sub-25 nm vias and trenches in polymers," *Appl. Phys. Lett*ers, vol. 67, pp. 3114, 1995.

[2] Akter, T., Desai, S., "Developing a Predictive Model for Nanoimprint Lithography using Artificial Neural Networks," *Materials and Design,* vol. 160, no. 15, pp. 836-848, 2018.

[3] Almakaeel H., Albawali A., Desai S., "*Artificial neural network based framework for cyber nano manufacturing," Manufacturing Letters*, vol. 15, part B, pp. 151-154, 2018.

[4] Desai S., Craps M., Esho T., "Direct Writing of Nanomaterials for Flexible Thin Film Transistors (fTFTs)," *The International Journal of Advanced Manufacturing Technology*, vol. 64, no. 1, pp. 537-543. 2013.

[5] T. Köpplmayr, L. Häusler, I. Bergmair, and M. Mühlberger, "Nanoimprint Lithography on curved surfaces prepared by fused deposition modeling," *Surface Topography: Metrology and Properties*, vol. 3, no, 2, p 024003, 2015.

[6] Gaikwad, A. and S. Desai, "Understanding Material Deformation in Nanoimprint of Gold using Molecular Dynamics Simulation," *American J. of Engineering and Applied Sciences*, vol. 11, no. 2, pp. 837-844. 2018.

[7] Gaikwad A., Clarke A., Desai S., "Molecular Dynamics Study of the Quenching Effect on Direct Nanoimprint of Gold," *Proceedings of the Industrial Engineers Research Conference*, 2019, Orlando, FL.

[8] Cordeiro, J., & Desai, S., "The Nanoscale Leidenfrost Effect," *Nanoscale,* vol. 11, pp. 12139-12151, 2019.

[9] Marquetti I., Desai S., "Orientation Effects on the Nanoscale Adsorption Behavior of Bone Morphogenetic Protein-2 on Hydrophilic Silicon Dioxide," *RSC Advances*, vol. 9, pp. 906-916, 2019.

[10] Marquetti I., Desai S., "Molecular Modeling the Adsorption Behavior of Bone Morphogenetic Protein - 2 on Hydrophobic and Hydrophilic Substrates," *Chemical Physics Letters*, vol. 706. pp. 285-294, 2018.

[11] J. R. Rocha, K. Z. Yang, T. Hilbig, and W. Brostow, "Polymer indentation with mesoscopic molecular dynamics," *J. Mater. Res*., vol. 28, no. 2, pp. 3043-3052, 2013.

[12] K-H. Chang: Chapter 17 – Design Optimization. *e-Design Computer-Aided Engineering Design. Academic Press,* pp. 907-1000, 2015.

[13] Y. Chang and S-W. Chang, "Full-atomistic simulations of poly(ϵ-caprolactone) diol model with CVFF and CGenFF," *Multiscale and Multiphysics Mechanics*, vol. 1, no. 4, pp. 327-340, 2016.

[14] A. P. Awasthi, D. C. Lagoudas, and D. C. Hammerand, "Modeling of graphene-polymer interfacial mechanical behavior using molecular dynamics," *Modelling Simul. Mater. Sci. Eng*., vol. 17, pp. 015002, 2009.

[15] C. S. Brazen and S. L. Rosen: Fundamental Principles of Polymeric Material*s* 3rd Ed. *Wiley,* 2012.

[16] P. Dauberosguthorpe, V. A. Roberts, D. J. Osguthorpe, J. Wolff, M. Genest, and A.T. Hagler, "Structure and energetics of ligand binding to proteins: Escherichia coli dihydrofolate reductase-trimethoprim, a drug-receptor system," *Proteins: Structure, Function, and Bioinformatics*, vol. 4, no. 1, pp. 31-47, 1988.

[17] S. Plimpton: Fast parallel algorithms for short-range molecular dynamics. *Journal of Computational Physics*

[18] S. Alexander, "Visualization and analysis of atomistic simulation data with OVITO-the Open Visualization Tool," *Modeling and Simulation in Materials Science and Engineering*, vol. 18, no. 1, pp. 15012, 2010.

[19] MATLAB. Version 2019a. Natick, Massachusetts. *The MathWorks Inc*. (2019).

[20] Marquetti, I., J. Rodrigues, and S.S. Desai, "Ecological Impact of Green Computing Using Graphical Processing Units in Molecular Dynamics Simulations," *International Journal of Green Computing*, vol. 9, no. 1, pp. 35-48, 2018.